Yishen Jiangzhuo decoction attenuates cisplatin-induced acute kidney injury by inhibiting inflammation, oxidative stress and apoptosis through the TNF signal pathway

DENGYONG ZHENG[1,2], XINGLIN RUAN[3], QIANG WU[2], YULIANG QIU[4] and SHIWEI RUAN[4]

[1]Academy of Integrative Medicine, Fujian University of Traditional Chinese Medicine, Fuzhou, Fujian 350122;
[2]Department of Nephrology, The Second Affiliated People's Hospital of Fujian University of
Traditional Chinese Medicine, Fuzhou, Fujian 350003; [3]Department of Neurology, Fujian Medical University
Union Hospital, Fuzhou, Fujian 350001; [4]Department of Nephrology, People's Hospital Affiliated to
Fujian University of Traditional Chinese Medicine, Fuzhou, Fujian 350004, P.R. China

Abstract. The present study aimed to investigate the therapeutic effects and mechanisms of Yishen Jiangzhuo decoction (YSJZD) in a mouse model of cisplatin-induced acute kidney injury (AKI). The mice were divided into the NC, cisplatin and cisplatin + YSJZD groups. A concentration-dependent effect of YSJZD on cisplatin-induced AKI was observed and the optimal concentration for intervention was calculated. Changes in blood urea nitrogen and serum creatinine levels combined with hematoxylin and eosin and periodic acid-Schiff staining and transmission electron microscopy observations indicated that YSJZD enhanced renal function, reduced pathological injury and protected renal tubular epithelial cells in cisplatin-induced AKI mice. The results of the transcriptomic and enrichment analyses showed that the mechanisms of YSJZD may be associated with inflammation, oxidation, apoptosis and the TNF signal pathway. Immunofluorescence, oxidative stress index, terminal deoxynucleotidyl transferase dUTP nick end labeling assay and western blotting revealed that YSJZD downregulated apoptosis in the renal tissues of AKI mice and further decreased the expression levels of p-p65, p-p38 MAPK, TNF-α, cleaved-caspase-3 and malondialdehyde, while increasing the levels of NAD-dependent protein deacetylase sirtuin-3, glutathione and superoxide dismutase. Overall, the results showed that YSJZD could effectively abrogate cisplatin-induced AKI in mice through mechanisms primarily related to its anti-inflammatory, antioxidative and antiapoptotic effects by inhibited the TNF signal pathway. YSJZD warrants further investigation as a clinical empirical prescription.

Introduction

Cisplatin, also known as cis-diaminedichloroplatinum (CDDP), is an effective drug used to treat numerous types of cancer (1). However, cisplatin easily accumulates and is biotransformed in the kidneys (2), which can lead to serious side effects including acute kidney injury (AKI). Of patients treated with cisplatin, ~30% develop AKI (3). This serious side effect limits the clinical application of cisplatin (4).

Renal tubular epithelial cells (RTECs) are the primary cellular target in cisplatin-induced AKI (1,5). Cisplatin leads to the injury and death of RTECs by activating complex signaling pathways, including apoptosis, necrosis, inflammation and increased oxidative stress (6). Further, cisplatin promotes the activation and cytosol-to-nucleus translocation of nuclear factor (NF)-κB, in addition to promoting the production of inflammatory cytokines and chemokines. This pathway contributes to cisplatin-induced nephrotoxicity by increasing the production of TNF-α in renal tubular cells (7,8). Furthermore, cisplatin alters mitochondrial metabolism and produces reactive oxygen species (ROS). Cisplatin-induced AKI is associated with increased ROS production in the renal proximal convoluted tubular cells (9) and AKI development has been shown to depend on cell death. Cisplatin induces necrosis and the intrinsic, extrinsic and endoplasmic reticulum (ER) stress-associated apoptosis pathways (10). Despite several decades of research, no stable drug treatment option is available to reduce the cisplatin-induced AKI, which poses a serious concern for patients receiving treatment with it (5).

Yishen Jiangzhuo decoction (YSJZD) is an empirical prescription developed by Professor Shiwei Ruan, a traditional Chinese medicine (TCM) doctor in Fujian Province, China, after extensive clinical practice. This therapeutic is primarily used to treat chronic renal failure (11). YSJZD is comprised of a variety of herbs; False Starwort root, Milkvetch root, Large-headed Atractylodes rhizome, Poria, Mistletoe, Mulberry fruit, Achyranthes, Danshen, Chinese Angelica, Rhubarb, Serissa foetida, Plantain seeds and Tangerine peel. each of which contributes to its therapeutic effect, thus 'invigorating the kidney and spleen, reducing turbidity and removing blood stasis' in TCM terms (11).

The present study investigated the effect of YSJZD on a cisplatin-induced AKI mouse model and examined the effects of the optimal YSJZD concentration on renal function, pathology and tubular epithelial cell ultrastructure in cisplatin-induced AKI mice. The possible targets of YSJZD in cisplatin-induced AKI in mice were identified by transcriptome sequencing and differential expression analysis. The protective effects of YSJZD against cisplatin-induced AKI and its primary mechanism of action were revealed *in vivo*, thus providing theoretical and experimental support for the therapeutic treatment of cisplatin-induced AKI with YSJZD.

Materials and methods

Drug preparation. In the first round of preparation, the thirteen herbs present in YSJZD (Table I) were soaked in purified water for 1 h. The nascent decoction was initially boiled at high heat, then simmered and decocted for 30 min. The decoction was then removed from heat. In the second step, the herbs were soaked for 10 min, after which they were processed following the same steps as in the first round. The second decoction was mixed with the first. The combined solution was filtered thrice through four layers of sterile surgical gauze. After filtering, the solution was decocted over low heat and alternately concentrated to volumes of 300, 150 and 75 ml, corresponding to herb solutions of 0.7, 1.4 and 2.8 g/ml raw medicine. The equivalent dose ratio of mice to 70 kg adults was 9.1. The dose calculation (209 g ÷ 70 kg x 9.1 = 27.17 g/kg) indicated a working dose of 28 g/kg, following the pharmacological experimental methodology described by Xu *et al* (12). Cisplatin injection was obtained from Jiangsu Hausen Pharmaceutical Group Co Ltd. (cat. no. H20040813).

Construction of the cisplatin-induced AKI murine model. A total of 181 specific pathogen-free male ICR mice aged 7-8 weeks were purchased from the Laboratory Animal Center of Fujian Medical University [Certificate No. SCXX (Min) 2016-0002]. Mice were housed with free access to food and water under controlled environmental conditions (temperature 22±2˚C; humidity 50-60%; 12-h light/dark cycle). The health and behavior of mice were observed twice a day. The mice were adaptively fed for 7 days and weighed 29-33 g at the time of the experiment. The experimental protocols (approval no. FJ-TCM IACUC2020021) were approved by the Fujian University of Traditional Chinese Medicine Laboratory Animal Welfare and Ethics Committee. Fig. S1 gives a flow chart of the experiments detailed below.

Mortality rates of mice induced by different doses of cisplatin. A total of 40 mice were divided into cisplatin 20, 18.75, 18, 15, 0 mg/kg groups (n=8) and the cisplatin induced AKI model was established by intraperitoneal injection of corresponding cisplatin solution, the 10-day mortality of mice in 5 groups was observed. 20 and 18.75 mg/kg cisplatin, which had the higher mortality rates, were selected as the modeling doses of CDDP for follow-up experiments. See 'Effects of YSJZD on the survival rate of cisplatin-induced AKI mice'.

Effects of YSJZD on the survival rate of cisplatin (20 mg/kg)-induced AKI mice. A total of 40 mice were divided into 4 groups (n=10), as follows: i) cisplatin, ii) cisplatin + YSJZD (7 g/kg), iii) cisplatin + YSJZD (14 g/kg), iv) cisplatin + YSJZD (28 g/kg). A single intraperitoneal injection of 20 mg/kg of cisplatin was used to establish the model of cisplatin-induced AKI in mice. Intragastric administration corresponding concentrations of YSJZD began 30 min before modeling and continued once daily at the same time after modeling. The cisplatin group was administered the corresponding dose of purified water. The 10-day mortality of mice in 4 groups was observed. The survival rate of mice in the cisplatin 20 mg/kg + YSJZD 14 g/kg group was the highest; however, no statistically significant difference was noted. The intraperitoneal injection of 20 mg/kg cisplatin solution in mice resulted in a high mortality rate; therefore, the dose of cisplatin was subsequently reduced to 18.75 mg/kg. See 'Effects of YSJZD on the survival rate of cisplatin-induced AKI mice'.

Effects of YSJZD on the survival rate of cisplatin (18.75 mg/kg)-induced AKI mice. A total of 45 mice were divided into 3 groups (n=15), as follows: i) cisplatin, ii) cisplatin + YSJZD (7 g/kg), iii) cisplatin + YSJZD (14 g/kg). A single intraperitoneal injection of 18.75 mg/kg of cisplatin was used to establish the model of cisplatin-induced AKI in mice. Intragastric administration corresponding concentrations of YSJZD began 30 min before modeling and continued once daily at the same time after modeling. The cisplatin group was administered the corresponding dose of purified water. The 15-day mortality of mice in three groups was observed.

Short-term effects of YSJZD on hepatotoxicity in mice. A total of 16 mice were divided into Normal control and YSJZD groups (n=8) in a toxicological experimental. YSJZD group was Intragastric administration of YSJZD 14 g/kg for 4 days, The Normal control group was administered the corresponding dose of purified water, then blood taken for alanine aminotransferase (ALT) detection.

Effects of YSJZD therapy in cisplatin (18.75 mg/kg)-induced AKI mice. A total of 40 mice were divided into five groups, as follows: i) Normal control (NC; n=8), ii) cisplatin 2-days (n=8), iii) cisplatin 4-days (n=8), iv) cisplatin + YSJZD 2-days (n=8) and v) cisplatin + YSJZD 4-days (n=8). A single intraperitoneal injection of 18.75 mg/kg of cisplatin was used to establish the model of cisplatin-induced AKI in male ICR mice. Mice in the NC group (n=8) were injected with corresponding doses of saline. In the treated mice, YSJZD (14 g/kg) was administered intragastrically 30 min before modeling and continued daily after modeling. The model and NC groups were administered

Table I. Components of Yishen Jiangzhuo decoction.

Latin binominal	English name	Part used	Origin of product (province)	Type of product	Weight (g)
Viscum sp.	Mistletoe	Leaf with stem branch	Heilongjiang	Raw (dry)	15
Mori albae	Mulberry fruit	Fruit	Anhui	Raw (dry)	15
Achyranthes bidentata	Achyranthes root	Root	Henan	Raw (dry)	15
Pseudostellaria heterophylla	False Starwort root	Root	Fujian	Raw (dry)	15
Atractylodes macrocephala	Large-headed Atractylodes rhizome	Stem	Zhejiang	Raw (dry)	15
Poria cocos	Poria	Sclerotium	Hubei	Raw (dry)	15
Astragalus	Milkvetch Root	Root	Gansu	Raw (dry)	30
Angelicae sinensis	Chinese angelica	Root	Gansu	Raw (dry)	10
Citri reticulatae	Tangerine peel	Peel	Guangdong	Raw (dry)	10
Plantaginis	Plantain Seed	Seed	Sichuan	Raw (dry)	15
Salviae miltiorrhizae	Danshen Root	Root	Shandong	Raw (dry)	30
Rheum	Rhubarb	Root and rhizome	Sichuan	Raw (dry)	9
Serissa japonica (Thunb.)	Serissa Foetida	Whole herb	Hubei	Raw (dry)	15

corresponding doses of purified water. After 2 and 4 days, the mice were anesthetized by intraperitoneal injection of pentobarbital sodium (50 mg/kg) and blood was then taken from the heart (~200 μl per mouse). Then the mice were sacrificed by intraperitoneal injection of pentobarbital sodium (150 mg/kg). After the mice had cardiac and respiratory arrest and showed no nerve reflex, the kidneys were taken for further study. The mice demonstrated the following humane endpoints: The mice continued to lie down and there was a loss of righting reflex. In addition, a toxicological experimental group was set up to give YSJZD 14 g/kg for 4 days and then blood taken from the heart for alanine aminotransferase (ALT) detection following anesthesia and then sacrifice as aforementioned. Blood samples were collected to assess renal function and ALT. A section of kidney tissue was harvested for paraffin embedding and electron microscopy. The other section of the kidney tissues were stored at -80˚C for transcriptome sequencing, differential expression and molecular analyses.

Renal function detection. Serum creatinine (SCr), blood urea nitrogen (BUN) and ALT levels were measured using an automated biochemical analyzer (Abbott Cil6200; Abbott Laboratories).

Renal pathological observation. The fixed kidney tissue was dehydrated by gradient alcohol, cleared with xylene and embedded with paraffin. Paraffin sections (4 μm) were stained with hematoxylin and eosin (H&E) and periodic acid-Schiff (PAS) stains. H&E was staining with hematoxylin for 5 min and eosin for 2 min at room temperature. PAS was staining with periodic acid for 10 min and Schiff's solution for 10 min at room temperature. Renal damage was graded using kidney slices stained with H&E (n=8). Paller scores (13) were used to determine the degree of renal tubule damage in H&E-stained kidney sections (n=8) and the morphology was observed under a light microscope. A total of 10 non-overlapping renal tissue fields (magnification, x200) and 10 renal tubules were randomly selected from each field. In total, 100 renal tubules from each mouse were evaluated. The severity of renal tubular damage was assessed by assigning points based on specific criteria: Renal tubular dilatation and flattened tubular epithelial cells and renal tubular epithelial brush border damage were assigned one point each and shedding was assigned two points. Cast formation in renal tubules was assigned two points and exfoliative and necrotic cells in the lumen of renal tubules (without cast formation or cell fragments) were scored at one point each. The maximum possible score was five points. Higher scores indicated more severe damage to the renal tubules.

Transmission electron microscopy. A total of three cortical kidney tissue samples were randomly selected from each group. Kidney cortex tissues were fixed in 2.5% glutaraldehyde (cat. no. G1102; Wuhan Servicebio Technology Co., Ltd.) for 4 h at 4˚C and 1% osmic acid (cat. no. 18466, Ted Pella Inc.) for 2 h at room temperature to examine the ultrastructural alterations in the proximal tubular epithelial cells. Subsequently, samples were dehydrated using a gradient of alcohol and acetone and embedded in 812 epoxy resin. Following ultrathin sectioning, the tissues were stained with lead citrate (cat. no. 19312; Ted Pella Inc.) and uranyl acetate (cat. no. 19481; Ted Pella Inc.). Transmission electron microscopy was applied to identify stained slices (HT-7700; Hitachi, Ltd.). Image information acquisition using Transmission electron Microscopy imaging system (Hitachi TEM system; Hitachi, Ltd.).

RNA extraction and RNA quantitative and quality detection. A total of three cortical kidney tissue samples were randomly selected from each group. Total ribonucleic acid (RNA) was

isolated from 50 mg of kidney tissue using 1 ml of Trizol reagent (cat. no. B610409-0100; Sangon Biotech Co., Ltd., Shanghai, China), following the manufacturer's instructions. An Agilent 5300 Fragment Analyzer (Agilent Technologies Inc.) was used to perform quantitative and quality RNA detection, comprising elucidation of concentration, RNA integrity number (RIN) and 28 S to 18 S ratio (28S/18S). A RIN value close to 10 indicates high sample integrity. The 28 S/18 S is another indicator to evaluate sample integrity, for which a eukaryotic ratio ≥1.5 indicates good RNA integrity. Only high-quality whole RNA samples were used to generate complementary deoxyribonucleic acid (cDNA) libraries.

RNA-seq and cDNA library creation. BGI Shenzhen Co., Ltd. prepared a cDNA library and performed RNA-Seq on a DNBSEQ platform (BGI Shenzhen Co., Ltd.) in accordance with the manufacturer's instructions.

Bioinformatics analysis. Bioinformatics analysis tools, including SOAPnuke (v1.5.6, https://github.com/BGI-flexlab/SOAPnuke), FastQC (v0.11.7, http://www.bioinformatics.babraham.ac.uk/projects/fastqc/), HISAT2 (v2.1.0, http://www.ccb.jhu.edu/software/hisat), Bowtie2 (v2.3.4.3, http://bowtie-bio.sourceforge.net/index.shtml), RSEM (v1.3.1, http://deweylab.biostat.wisc.edu/rsem), DESeq2 (v1.4.5, http://www.bioconductor.org/packages/release/bioc/html/DESeq2.html) and Phyper function in R package v 2.26.0 (http://github.com/jdstorey/qvalue), were employed in the present study. Low-quality raw reads were removed using the BGI SOAPnuke filtering program. The quality of the clean reads was assessed using the FastQC software and the sequencing quality values Q20 and Q30 were calculated to determine whether the sequencing data were sufficient for subsequent analysis. The HISAT2 software was used to match clean reads to the mouse reference genome and to check whether the mapping outcomes satisfied the calibrated quality control. Clean reads were aligned to reference gene sequences using Bowtie2 software and the gene expression levels of each sample were calculated using RSEM software. The fragments per kilobase of transcripts per million mapped fragments (FPKM) was calculated to evaluate the transcript expression levels for each sample. Typically, a transcript was considered to be expressed if its FPKM value was >0.1. DESeq2 software was used to identify differentially expressed genes (DEGs) between groups, with the threshold set at a fold-change threshold ≥2 and a Q-value <0.05. Kyoto Encyclopedia of Genes and Genomes (KEGG) pathway enrichment and Gene Ontology (GO) enrichment analyses of DEGs were performed using the phyper function in R code.

Immunofluorescence. For immunofluorescence analysis, paraffin sections were incubated with the following antibodies at 4˚C overnight: Anti-Phospho-p65 (1:200; Cell Signaling Technology (CST); cat. no. 3033), then goat anti-rabbit IgG Alexa Fluor 594 (1:200; Proteintech Group, Inc.; cat. no. SA00006-4) for 1 h. Following DAPI counterstaining for 10 min at room temperature, the sections were examined under a fluorescence microscope (EVOS M5000 Cell Imaging System; Invitrogen; Thermo Fisher Scientific, Inc.).

TdT-mediated dUTP nick end labeling (TUNEL) assay. Apoptosis in kidney sections was determined using an *in situ* cell death detection kit (Roche Diagnostics GmbH), in accordance with the manufacturer's recommendations. Briefly, the sections were deparaffinized in xylene, rehydrated with decreasing grades of ethanol and permeabilized with proteinase K at a concentration of 20 μg/ml in 10 mM Tris-HCl (pH 7.4-8) for 30 min at room temperature. The slices were then washed and incubated in the TUNEL reaction mixture at 37˚C for 1 h. DAPI was used as a nuclear counterstain for 10 min at room temperature. Images were captured using an EVOS M5000 Cell Imaging System (Invitrogen; Thermo Fisher Scientific, Inc.) A total of six randomly selected fields (magnification, x200) from each kidney were counted to determine the number of TUNEL-stained apoptotic renal tubular epithelial cells. ImageJ software (version 1.49; National Institutes of Health) was used to analyze the images.

Determination of glutathione (GSH), superoxide dismutase (SOD) and malondialdehyde (MDA) levels. Kidney tissue was homogenized and lysed, after which samples were centrifuged at 1,120 x g for 10 min at 4˚C. The levels of GSH, SOD and MDA in the supernatant were measured using commercial GSH, SOD (Nanjing Jiancheng Bioengineering Institute) and MDA (Beyotime Institute of Biotechnology) assay kits, respectively, according to the manufacturer's instructions.

Western blotting (WB) assay. Renal tissue was added to ice-cold RIPA lysis buffer (Beyotime Institute of Biotechnology) and homogenized using a tissue homogenizer (IKA Werke GmbH & Co. KG) at speed in second gear under cold conditions. An ultrasonic cell processor (Sonics & Materials, Inc.) was used to apply ultrasound for 5 sec x 3 times at 30% power on ice (20 KHz, with intervals of 10 sec). Protein concentrations were determined using a bicinchoninic acid (BCA) protein assay kit (Pierce; Thermo Fisher Scientific, Inc.). Subsequently, total protein samples were adjusted to the same concentration and a loading buffer was added to the samples before boiling for 10 min at 100˚C to denature them. Protein samples (30 μg per lane) were then separated on a 10 or 15% sodium dodecyl sulfate-polyacrylamide gel electrophoresis (SDS-PAGE) separator and subsequently transferred to a 0.22 μm polyvinylidene fluoride (PVDF) membrane (MilliporeSigma). The PVDF membranes were blocked for 1 h at room temperature with 5% nonfat milk in PBST (PBS + 0.05% Tween-20). Membranes were then treated with the following antibodies overnight at 4˚C: Anti-TNFα antibody (1:1,000; Abcam; cat. no. ab215188), anti-Phospho-p65 antibody p65 (1:1,000; Ser536; CST; cat. no. 3033), anti-p65 (1:1,000; CST; cat. no. 8242), anti-p38 antibody (phospho T180+Y182) (1:1,000; Abcam; cat. no. ab195049), anti-p38 mitogen-activated protein kinase (MAPK; 1:1,000; CST; cat. no. 8690), anti-caspase 3/P17/P19 (1:500; Proteintech Group, Inc.; cat. no. 19677-1-AP), anti-Sirt3 (1:1,000; Abcam; cat. no. ab246522) and anti-β-actin (1:1,000; Santa Cruz Biotechnology, Inc.; cat. no. sc-47778). Membranes were then exposed to appropriate secondary horseradish peroxidase-conjugated antibodies for 1 h at room temperature and observed using an ultrasensitive electrochemiluminescence kit (Beyotime Institute of Biotechnology). An iBright1500 imaging system (Invitrogen; Thermo Fisher Scientific, Inc.)
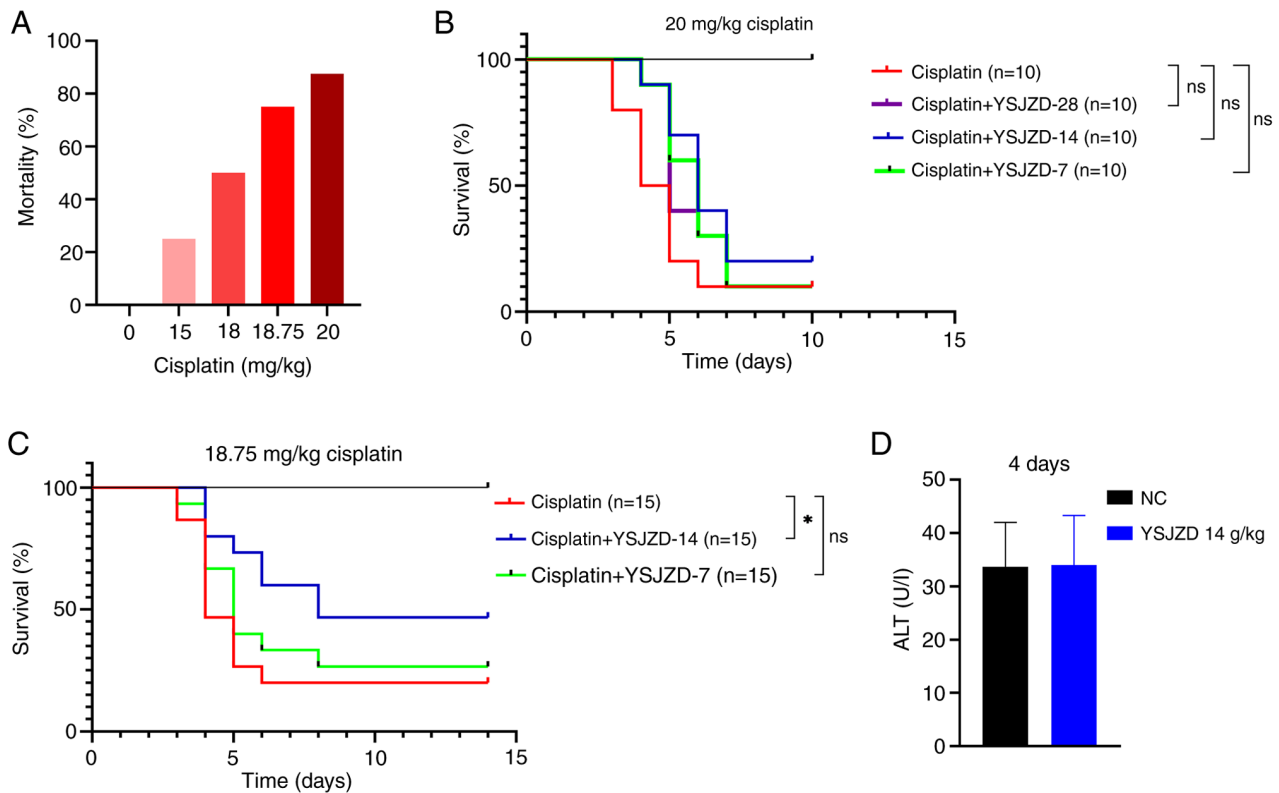
Figure 1. Effects of YSJZD on the survival rate of cisplatin-induced AKI mice. (A) Mortality rates of mice induced by different doses of cisplatin (n=8). (B) Effects of YSJZD on the survival rate of cisplatin (20 mg/kg)-induced AKI mice (n=10). (C) Effects of YSJZD on the survival rate of cisplatin (18.75 mg/kg)-induced AKI mice (n=15). (D) Short-term effects of YSJZD on hepatotoxicity in mice (n=8). *P<0.05 vs. the cisplatin group. ns, not significant; YSJZD, Yishen Jiangzhuo decoction; AKI, acute kidney injury; NC, normal control.

was used to detect signals and ImageJ software (version 1.51j8; National Institutes of Health) was used to quantify the band intensities.

Statistical analyses. Data analyses were performed using GraphPad Prism 8.0 (Dotmatics) or SPSS software (version 22.0; IBM Corp.). Normally distributed data are expressed as the mean ± standard deviation and were analyzed using a one-way analysis of variance (ANOVA) and Tukey's post hoc test. For non-normally distributed data, the Kruskal-Wallis test was used. P<0.05 was considered to indicate a statistically significant difference.

Results

Effects of YSJZD on the survival rate of cisplatin-induced AKI mice. In the present study, The mortality rates in the 20, 18.75, 18 and 15 mg/kg cisplatin groups (n=8 each) were 87.5, 75, 50 and 25%, respectively (Fig. 1A). Therefore, 20 and 18.75 mg/kg, which had the higher mortality rates, were selected as the modeling doses of CDDP for follow-up experiments.

As shown in Fig. 1B, the survival rate of mice in the cisplatin + YSJZD 14 g/kg group was the highest; however, no statistically significant difference was noted between the two groups. The intraperitoneal injection of 20 mg/kg cisplatin solution in mice resulted in a high mortality rate; therefore, the dose of cisplatin was subsequently reduced to 18.75 mg/kg. YSJZD at 28 g/kg concentration was no more effective in improving survival rates than concentrations of

14 and 7 g/kg, and was therefore excluded from further experiments. The cisplatin (18.75 mg/kg)-induced AKI mouse model was selected for future investigations of the effect of YSJZD on the survival rate of these mice and YSJZD 14 g/Kg and YSJZD 7 g/Kg were selected for medication intervention.

As shown in Fig. 1C, the survival rate of the cisplatin + YSJZD 14 g/kg group was significantly higher than that of the cisplatin group (P<0.05). The cisplatin + YSJZD 7 g/kg group had a higher survival rate than the model group (P<0.05). Based on these results, the YSJZD concentration of 14 g/kg was selected for subsequent experiments to observe its effects on the indices of cisplatin (18.75 mg/kg)-induced AKI.

Fig. 1D demonstrates that short-term YSJZD administration has no hepatotoxicity in normal unrestricted diet mice (n=8). No mice died except in the cisplatin group and cisplatin + YSJZD group in the mortality observation experiment. In the cisplatin 4-day group and cisplatin + YSJZD 4-day group, one mouse in each group was harvested blood and kidney and sacrificed at 84-96 h due to humane endpoint being reached.

Effect of YSJZD on renal function, renal pathology and renal tubular epithelial cell ultrastructure in mice with cisplatin-induced AKI. Serum BUN and SCr levels in the model group were significantly higher than those in the NC group on the second day following AKI induction (P<0.01). Compared with the cisplatin group, the serum BUN and SCr levels in the cisplatin + YSJZD group were reduced; however, the difference did not reach significance. On the fourth day following AKI, serum BUN and SCr levels were significantly higher
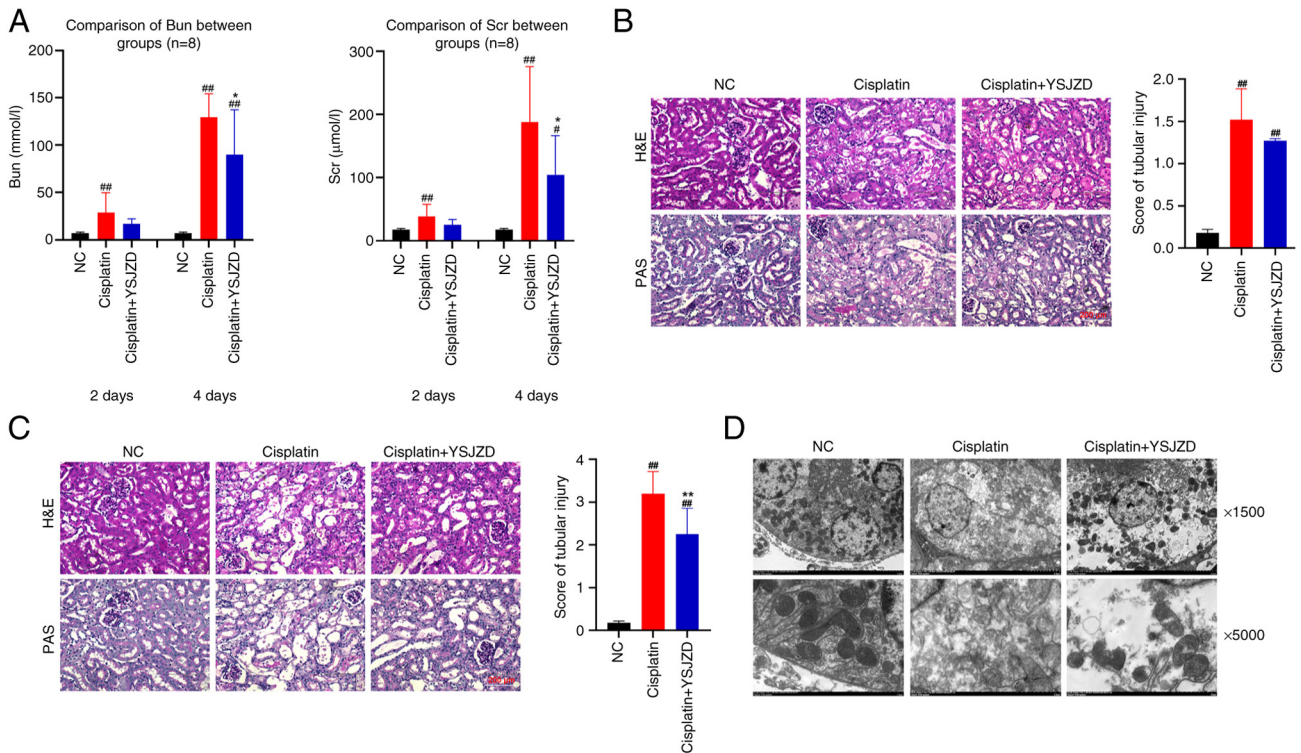
Figure 2. Effect of YSJZD on renal function, pathology and tubular epithelial cell ultrastructure in mice with cisplatin-induced AKI. (A) The effects of YSJZD therapy for 2 and 4 days on BUN (left panel) and SCr levels (right panel) in cisplatin-induced AKI mice (n=8). The results are from 2-day and 4-day groups. (B) Effect of a 2-days course of YSJZD therapy on the renal pathology (left panel) and the renal tubular damage score (right panel) of mice with cisplatin-induced AKI (n=8; magnification, x200; Scale bar, 200 μm). (C) Effect of a 4-days course of YSJZD therapy on the renal pathology (left panel) and the renal tubular damage score (right panel) of mice with cisplatin-induced AKI (n=8). (In left panel of C, the top three images show H&E staining. The bottom three images showed PAS staining. Images were acquired using a microscope at 200x magnification. Scale bar, 200 μm). (D) Effect of YSJZD treatment for 4 days on the ultrastructure of renal tubular epithelial cells in cisplatin-induced AKI mice (n=3). Images were acquired at x1,500 and x5,000 under transmission electron microscopy. The top three pictures are x1,500; the bottom three pictures are x5,000. #P<0.05, ##P<0.01 vs. NC group; *P<0.05, **P<0.01 vs. the cisplatin group. YSJZD, Yishen Jiangzhuo decoction; AKI, acute kidney injury; BUN, blood urea nitrogen; SCr, serum creatinine; H&E hematoxylin & eosin; PAS, periodic acid-Schiff; NC, normal control.

in the cisplatin group than in the NC group (P<0.01), while the serum BUN and SCr level was significantly lower in the cisplatin + YSJZD group than in the model group (P<0.05). The results revealed that YSJZD reduced serum BUN and SCr levels and improved renal function in cisplatin-induced AKI mice (Fig. 2A).

H&E and PAS staining of renal tissues treated with 14 g/kg YSJZD for 2 and 4 days revealed that the kidney tissue of the NC group exhibited a well-structured appearance with morphologically normal renal tubules and a regular cell arrangement. In the cisplatin group treated for 2 days, focal shedding of renal tubular epithelial cells, brush border shedding, slight dilation of the lumen, thinning of the renal tubular wall and tubular cast formation were observed in the renal cortex. The renal tubular damage score of the cisplatin group was higher than that of the NC group (P<0.01). Renal tubular epithelial cell shedding, lumen dilatation and cast formation were marginally improved in the cisplatin + YSJZD group compared to the cisplatin group. The renal tubular injury score in the cisplatin + YSJZD group was lower than that in the cisplatin group; however, this difference was not statistically significant (Fig. 2B).

After 4 days of modeling, renal tubular epithelial cells in the cisplatin group showed diffuse shedding, a disordered arrangement of renal tubular epithelial cells, significant lumen

dilatation, wall thinning, naked basement membrane and an abundance of tubular casts in the renal cortex of the cisplatin group. The renal tubular injury score in the cisplatin group was significantly higher in the cisplatin group than that in the NC group (P<0.01). Compared with the cisplatin group, the cisplatin + YSJZD group showed significantly reduced shedding of renal tubular epithelial cells, lumen dilation and tubular casting. Furthermore, the cisplatin + YSJZD group showed a significantly lower score (P<0.01). These findings demonstrated that YSJZD considerably ameliorated renal pathological alterations and lowered the renal tubular damage score in cisplatin-induced AKI mice (Fig. 2C).

Transmission electron microscopy was performed to examine the effect of 4-days-YSJZD treatment on the ultrastructure of renal tubular epithelial cells in cisplatin-induced AKI mice. As shown in Fig. 2D, electron microscopy revealed that the mitochondria of renal tubular epithelial cells in the cisplatin group were significantly reduced and the cytoplasm and organelles were disordered. By contrast, the cisplatin + YSJZD group showed significantly decreased ultrastructural damage to the cells. Thus, YSJZD alleviated damage to the ultrastructure of renal tubular epithelial cells and protected mitochondria in cisplatin-induced AKI mice.

GO and KEGG pathway enrichment analysis of DEGs in cisplatin-induced AKI mice following YSJZD therapy. To
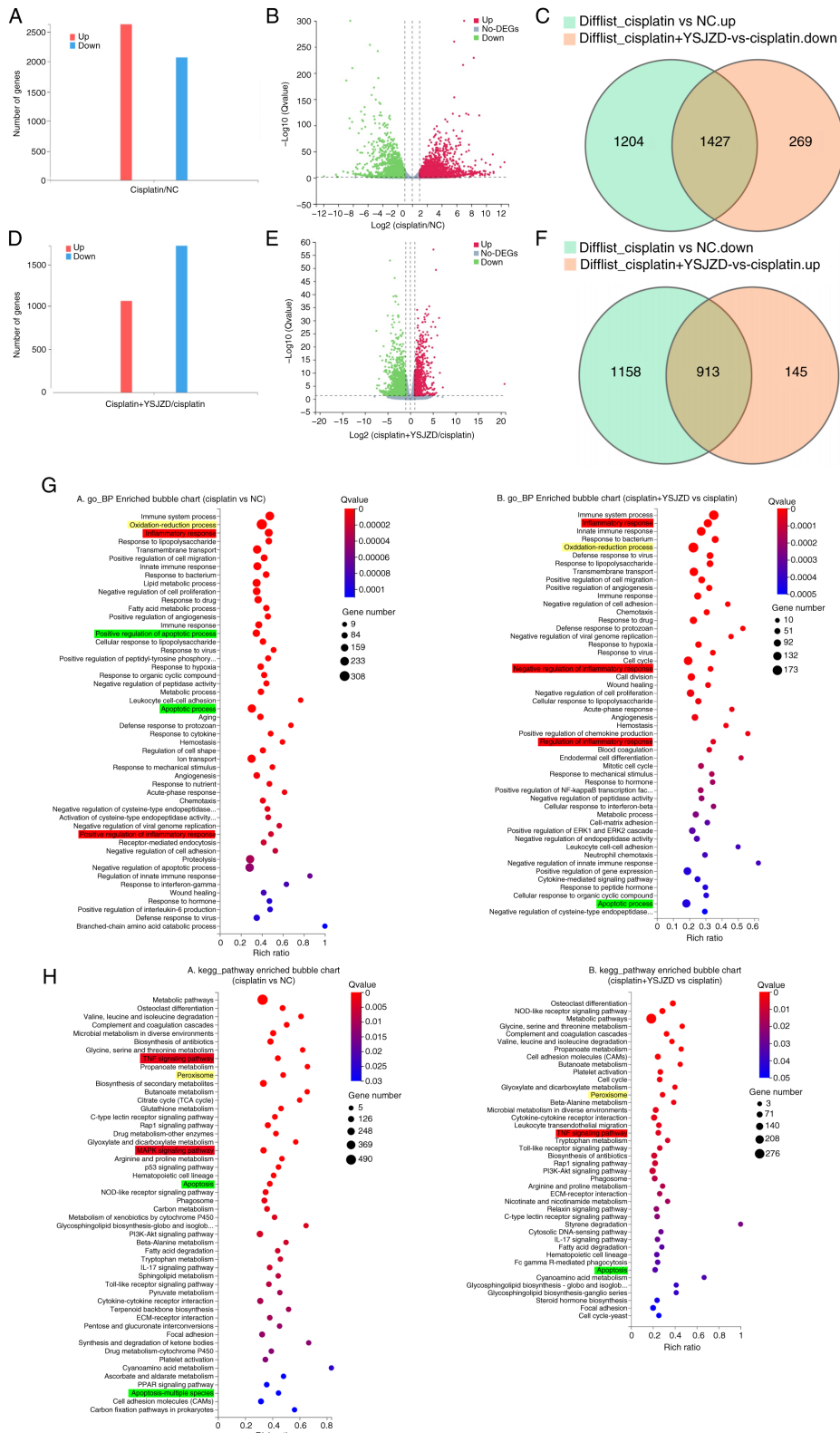
Figure 3. GO and KEGG pathway enrichment analysis of DEGs in cisplatin-induced AKI mice following YSJZD therapy. (A) DEGs in the cisplatin group compared with those in the NC group are shown as bar graphs with the number of related DEGs on the Y-axis. (B) Volcano plot of DEGs in the cisplatin group compared with the NC group; the X-axis is log2(fold change) and the Y-axis is -log10 (Q-value). (C) Downregulated DEGs in the cisplatin + YSJZD group compared to the cisplatin group, intersecting with upregulated DEGs in the cisplatin group compared to the NC group. (D) Bar chart of DEGs in the cisplatin + YSJZD group compared to the cisplatin group; number of corresponding DEGs in Y-axis. (E) Volcano plot of DEGs in the cisplatin + YSJZD group compared to those in the cisplatin group. (F) Upregulated DEGs in the cisplatin + YSJZD group compared to the cisplatin group, intersecting with downregulated DEGs in the cisplatin group compared to the NC group. (G) GO_ BP-enriched bubble charts of DEGs in comparison groups. (H) KEGG pathway enrichment bubble charts of DEGs in the comparison groups. The X-axis represents the rich ratio and the Y-axis represents the GO or KEGG terms. The bubble size represents the number of DEGs in a GO term or KEGG pathway, the color represents the Q-value; red represents a smaller Q-value and blue represents a larger Q-value. Red, yellow and green represent inflammatory response, oxidative stress and apoptotic processes or pathways, respectively. GO, Gene Ontology; KEGG, Kyoto Encyclopedia of Genes and Genomes; DEGs, differentially expressed genes; AKI, acute kidney injury; YSJZD, Yishen Jiangzhuo decoction; NC, normal control; BP, biological processes.

identify DEGs, a threshold of fold change ≥ 2 and Q-value < 0.05 was used. The selected DEGs were plotted as bar graphs and volcanic plots. In total, 4,702 DEGs were identified in the cisplatin group compared to the NC group, of which 2,631 were upregulated and 2,071 were downregulated (Fig. 3A and B). Additionally, 2,754 DEGs were identified when comparing the cisplatin + YSJZD group and the cisplatin group; of these, 1,058 were upregulated and 1,696 were downregulated (Fig. 3D and E).

Further analysis of the identified DEGs was conducted to determine the primary genes targeted by YSJZD in cisplatin-induced AKI. The intersection of upregulated DEGs after modeling and downregulated DEGs after YSJZD treatment identified 1,427 genes were downregulated following YSJZD treatment (Fig. 3C). The intersection of downregulated DEGs after modeling and upregulated DEGs after YSJZD treatment identified 913 genes upregulated after YSJZD treatment (Fig. 3F).

The primary biological functions of the candidate genes were determined by GO enrichment analysis. A comparison of DEGs between the cisplatin and NC groups using GO analysis revealed that 325 terms (Q-value <0.05) were enriched in biological processes (BP). The top 50 terms were selected to construct the bubble chart. The results showed enrichment in biological processes including the oxidation-reduction process, inflammatory response, positive regulation of the inflammatory response, apoptosis and positive regulation of apoptosis. Similarly, a comparison of the DEGs between the cisplatin and cisplatin + YSJZD groups using GO analysis revealed that 259 terms (Q-value <0.05) were enriched in biological processes. The top 50 terms were selected to create a bubble chart. The results showed enrichment in multiple pathways, including the oxidation-reduction process, inflammatory response, regulation of inflammatory response, negative regulation of inflammatory response and apoptosis (Fig. 3G).

The KEGG database was used as the primary accessible database for pathway analysis. The signaling pathways used by the potential genes were identified using KEGG pathway enrichment analysis. Fig. 3H shows the KEGG pathway enrichment analysis of the DEGs identified when the cisplatin and NC groups were compared. In total, 56 pathways showed significant changes (Q value < 0.05). The top 50 pathways were then selected to construct a bubble chart. Relevant signaling pathways were screened based on the results of the GO-BP analysis. Peroxisomes, TNF signaling, MAPK signaling, apoptosis and multiple forms of apoptosis were identified as the principal mechanisms involved. The DEGs identified in the comparison between the cisplatin + YSJZD and cisplatin groups were analyzed using KEGG pathway enrichment, with significant changes observed in 42 pathways (Q-value <0.05), which were subsequently visualized using a bubble chart. These pathways primarily involved the peroxisome, the TNF signaling pathway and apoptosis.

In summary, GO-BP enrichment of DEGs in the cisplatin vs. NC group and the cisplatin + YSJZD vs. cisplatin group was related to inflammation, oxidation-reduction processes and apoptosis. KEGG pathway enrichment of DEGs in the cisplatin vs. NC group and cisplatin + YSJZD vs. cisplatin group was also related to the inflammatory response, oxidative stress and apoptotic pathways. The raw RNA-seq data that support the findings were deposited in the gene expression omnibus (GEO) repository with an accession number GSE262792 (https://www.ncbi.nlm.nih.gov/geo/query/acc.cgi?acc=GSE262792.

Target genes of YSJZD in the treatment of cisplatin-induced AKI. GO-BP and KEGG pathway enrichment analysis of DEGs revealed the importance of pathways related inflammation, oxidative stress and apoptosis. Therefore, the signaling pathways involved were examined to identify the target genes that were affected by YSJZD therapy. As shown in Fig. 4A and C, the signaling pathway involved in central carbon metabolism in cancer involves the oxidative stress index, NAD-dependent protein deacetylase sirtuin-3 (SIRT3). It was observed that SIRT3 expression was downregulated in the model group and was upregulated following YSJZD treatment. Furthermore, in the TNF signaling pathway, TNF-α, NFκB and p38 MAPK were upregulated in the cisplatin group and downregulated following YSJZD treatment (Fig. 4B and D).

Effects of YSJZD on renal inflammatory indices in cisplatin-induced AKI mice. Compared with the NC group, a large amount of phosphorylated (p-)65 red fluorescence was observed in the nucleus of renal tubular epithelial cells in the cisplatin group and the p-p65 immunofluorescence intensity was significantly reduced following YSJZD treatment (Fig. 5A).

The WB results of p-p65, TNF-α and p-p38 MAPK in the renal tissue demonstrated that the p-p65/p65, TNF-α/β-actin and p-p38/p38 ratios of the cisplatin group were significantly greater than those of the NC group ($P<0.01$). The ratios of p-p65/p65, TNF-α/β-actin and p-p38/p38 in the cisplatin + YSJZD group were significantly lower than those in the cisplatin group ($P<0.05$; Fig. 5B-D). These findings demonstrate that YSJZD markedly reduced the expression levels of p-p65, TNF-α and p-p38 in the renal tissue of mice with cisplatin-induced AKI.

Effects of YSJZD on oxidative stress and apoptosis indices in cisplatin-induced AKI mice. The SIRT3/β-actin ratio in the cisplatin group was significantly lower than that of the NC group on WB data of renal tissue ($P<0.01$; Fig. 6A). Conversely, the SIRT3/β-actin ratio in the cisplatin + YSJZD group was significantly higher than that of the cisplatin group ($P<0.05$). These findings demonstrated that YSJZD substantially enhanced SIRT3 expression in the renal tissue of mice with cisplatin-induced AKI.

As shown in Fig. 6C, GSH and SOD activity levels in the cisplatin group were significantly lower than those in the NC group ($P<0.01$). MDA levels significantly increased in the cisplatin group ($P<0.01$). Similarly, GSH and SOD activity levels in the cisplatin + YSJZD group were significantly higher ($P<0.01$) than those in the cisplatin group, whereas MDA levels were significantly lower ($P<0.01$) in the cisplatin + YSJZD group. These findings demonstrated that YSJZD therapy greatly increased GSH and SOD levels in the renal tissue of cisplatin-induced AKI mice and markedly reduced MDA levels.

Compared with the NC group, the number of TUNEL-positive cells per field of renal tissue was significantly higher in the cisplatin group ($P<0.01$). Conversely, the number of TUNEL-positive cells per field in the cisplatin +
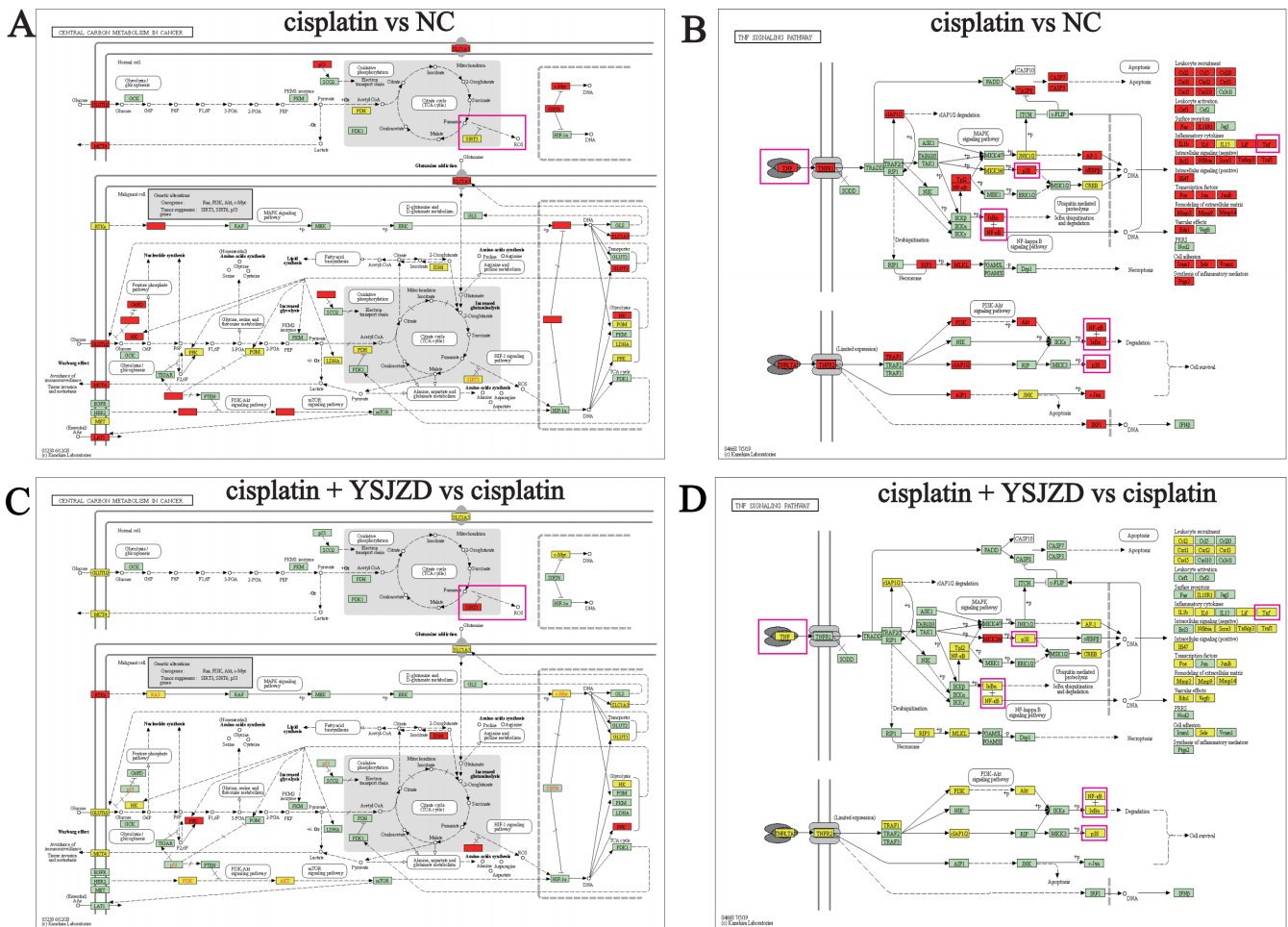
Figure 4. Changes in central carbon metabolism of cancer and the TNF signaling pathway map. (A) Changes in the central carbon metabolism of cancer cells in the cisplatin and NC groups. (B) Changes in the TNF signaling pathway in the cisplatin and NC groups. (C) Changes in the central carbon metabolism of cancer cells in the cisplatin + YSJZD vs. the cisplatin group. (D) Changes in the TNF signaling pathway in the cisplatin + YSJZD vs. the cisplatin group. Green represents background genes while red and yellow indicate DEGs with considerably elevated and decreased expression, respectively. NC, normal control; YSJZD, Yishen Jiangzhuo decoction; DEGs, differentially expressed genes.

YSJZD group was considerably lower than that in the cisplatin group (P<0.05) (Fig. 6B and D). As shown in Fig. 6E, the ratio of cle-caspase-3/caspase-3 in the cisplatin group was significantly higher (P<0.01) than that in the NC group, according to the WB findings of cle-caspase-3 in the renal tissue. The cle-caspase-3/caspase-3 ratio in the cisplatin + YSJZD group was significantly lower than that in the cisplatin group (P<0.05). These results revealed that YSJZD considerably reduced cisplatin-induced apoptosis of renal tubular epithelial cells in AKI mice.

Discussion

The clinical application of cisplatin or similar platinum-based treatments is commonly limited by the application of cisplatin-induced AKI. Complex processes underlie cisplatin-induced AKI, including the accumulation of cisplatin in renal tissue and the activation of inflammatory, oxidative and apoptotic pathways (5,14-16).

The present study found that the mortality rate of cisplatin-induced AKI mice was dose-dependent and that the 20 mg/kg cisplatin-induced mouse model had a high mortality rate. The mortality rate observed in the 20 mg/kg cisplatin-induced mouse model was similar to that observed by Linkermann et al (17). Therefore, the dose of cisplatin was reduced to 18.75 mg/kg. It was found that YSJZD reduces mortality in cisplatin-induced AKI mice. However, the YSJZD concentration of 28 g/kg was no improvement on 14 and 7 g/kg in terms of improving the survival rate, with the survival rate in the 14 g/kg group being the highest. Therefore, the optimal concentration of YSJZD was determined to be 14 g/kg. Furthermore, compared with the cisplatin group on the second day, the serum BUN and SCr levels in the cisplatin + YSJZD group were reduced; however, the difference was not statistically significant. This may be because the efficacy of YSJZD was time-dependent. YSJZD treatment for 4 days enhanced renal function and reduced pathological and renal tubular injury scores. YSJZD also protected RTECs against cisplatin-induced ultrastructural damage, particularly mitochondrial dysfunction. Overall, these results indicated that YSJZD was an effective drug for the treatment of cisplatin-induced AKI in mice.

YSJZD, a TCM compound with complex components, has multiple targets (11). Therefore, to elucidate its underlying mechanism of action, transcriptomic analysis was applied to analyze the effects of YSJZD. Subsequent GO-BP and KEGG
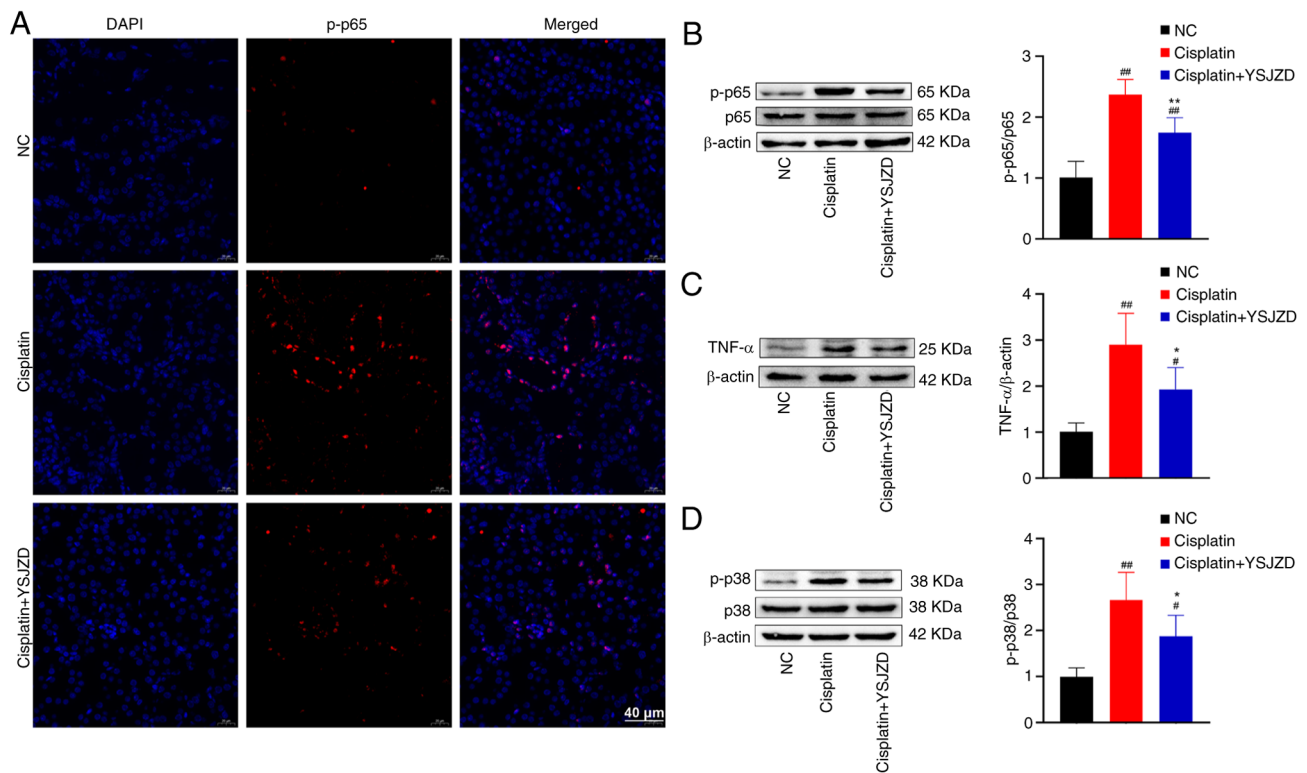
Figure 5. Effects of YSJZD on renal inflammatory indices in cisplatin-induced AKI mice. (A) Effect of YSJZD on immunofluorescent staining for p-p65 in the renal tissue of cisplatin-induced AKI mice. The renal tissue of each group displayed immunofluorescence for p-p65 (magnification, x400; scale bar, 40 μm). (B) Effect of YSJZD on p-p65 levels in the renal tissue of cisplatin-induced AKI mice. The bar chart shows the grey value ratio of p-p65 to p65 in the renal tissues of each group. (C) Effect of YSJZD on TNF-α in renal tissue of cisplatin-induced AKI mice. The bar chart shows the gray value ratio of TNF-α/β-actin in the renal tissue of each group. (D) Effect of YSJZD on p-p38 MAPK in the renal tissue of cisplatin-induced AKI mice. The bar chart shows the grey value ratio of p-p38 to p38 in the renal tissues of each group. #P<0.05, ##P<0.01 vs. the NC group; *P<0.05, **P<0.01 vs. the cisplatin group, n=5. YSJZD, Yishen Jiangzhuo decoction; AKI, acute kidney injury; p-, phosphorylated; NC, normal control.

pathway enrichment showed that the mechanisms of action of YSJZD may be related to inflammation, oxidation-reduction processes, apoptosis and the TNF signal pathway.

Cisplatin-induced AKI is strongly associated with the inflammatory response (8,18). Research has found that the activation of the NF-κB signaling pathway may be one of the primary mechanisms underlying cisplatin-induced AKI. Proximal tubular epithelial cells and immune cells infiltrating the kidney produce inflammatory cytokines (such as TNF-α) due to activation of the p65 pathway by cisplatin (2). Cisplatin causes the phosphorylation of p-p65 and its translocation from the cytosol to the nucleus (7). Inhibition of p65 transcriptional activity by an p65 inhibitor ameliorates cisplatin-induced AKI (19). Cisplatin nephrotoxicity is also significantly influenced by the p38 MAPK signaling pathway. The role of p38 MAPK in cisplatin-induced nephrotoxicity has been demonstrated both *in vitro* and *in vivo*. Pharmacological inhibitors of p38 (SB203580 and SKF-86002) were found to exert renoprotective effects in these models (7,20,21). The p38 MAPK pathway modulates TNF-α expression in renal tubular cells and the subsequent inflammatory response during cisplatin nephrotoxicity rather than directly controlling tubular cell damage and death (22). Thus, TNF-α plays a significant role in the pathophysiology of cisplatin-induced AKI (23). In the context of cisplatin nephrotoxicity, indigenous kidney cells, rather than invading inflammatory cells, create the majority of the TNF-α (24), Moreover, during cisplatin nephrotoxicity,

renal tubular cells considerably contribute to the generation of TNF-α (25). These inflammatory factors further induce inflammatory in renal tubular epithelial cells, leading to cell death and shedding, thus causing the onset and progression of AKI.

In the cisplatin-induced AKI mice in the present study, p-p65 red fluorescence was observed in the nuclei of renal tubular epithelial cells. The intensity of immunofluorescence was substantially diminished after treatment with YSJZD, thus indicating that YSJZD significantly reduced the expression level of p-p65 and TNF-α in the renal tissue of cisplatin-induced AKI mice. According to the results of WB for p-p65 and TNF-α in renal tissue, it was hypothesized that YSJZD decreased the renal inflammatory response in mice with cisplatin-induced AKI by reducing the phosphorylation and translocation of p65 into the nucleus and decreasing the expression level of TNF-α. Additionally, YSJZD significantly reduced the expression of p-p38 in the renal tissues of mice with cisplatin-induced AKI. The inhibition of p38 MAPK could also reduce the production of TNF-α, thus effectively protecting against cisplatin-induced kidney damage. These findings suggest that the anti-inflammatory activity of YSJZD is one of the mechanisms by which it alleviates cisplatin-induced AKI in mice.

Oxidative stress contributes significantly to cisplatin-induced nephrotoxicity (8). The increase in the endogenous antioxidant enzymes, GSH and SOD, in the renal tissue can
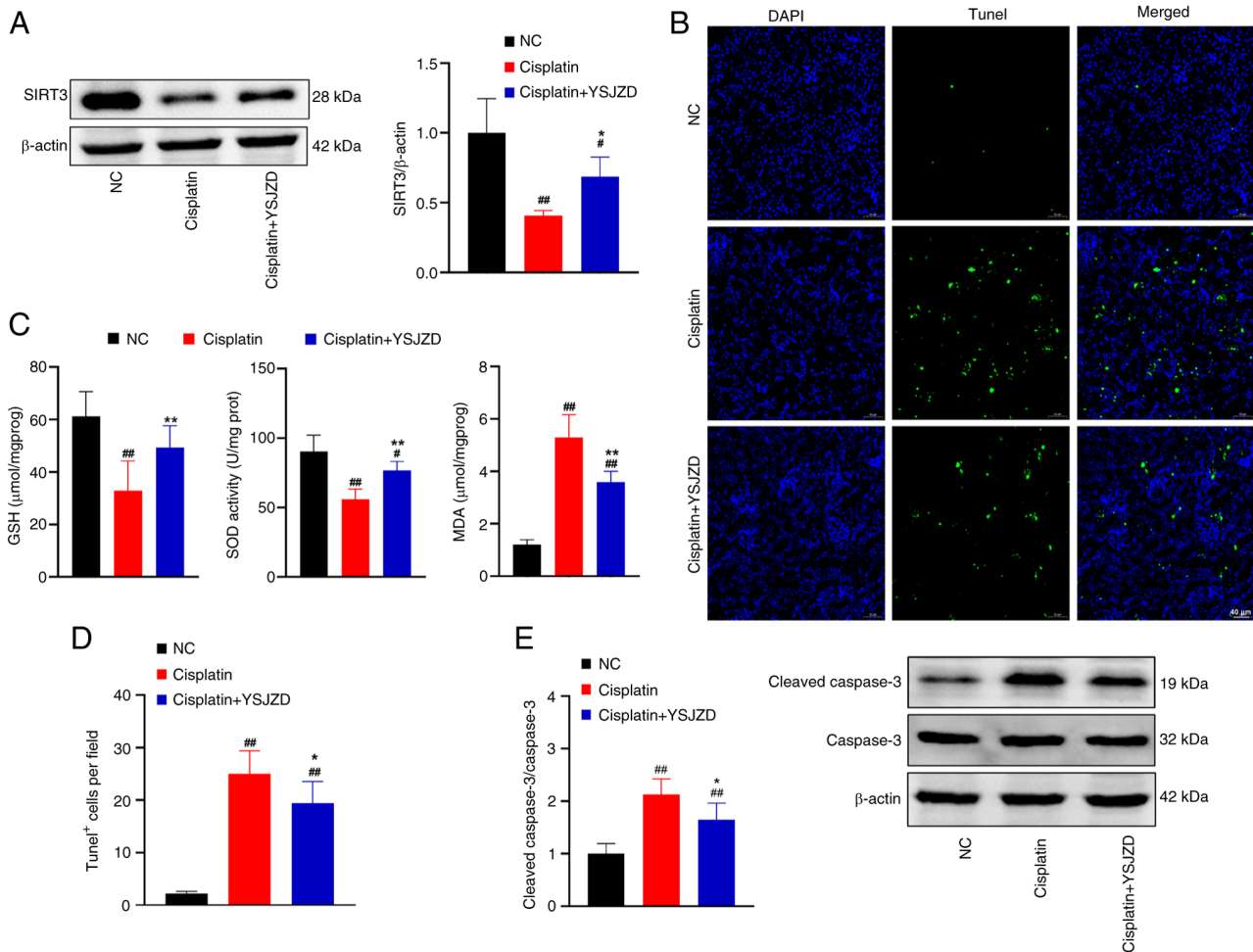
Figure 6. Effects of YSJZD on oxidative stress and apoptosis indices in cisplatin-induced AKI mice. (A) Effect of YSJZD on levels of SIRT3 in the renal tissue of cisplatin-induced AKI mice. The bar chart shows gray value ratio of SIRT3/β-actin in renal tissue of each group (n=5). (B) TUNEL fluorescence images of renal tissue in each group (magnification, x200; scale bar, 40 μm). (C) Effect of YSJZD on the GSH, SOD and MDA detection level in the renal tissue of cisplatin-induced AKI (n=8). (D) Statistical bar chart of TUNEL-positive cells per field of renal tissue for each group (n=8). (E) Effect of YSJZD on cleaved-caspase-3 in the renal tissue of cisplatin-induced AKI mice. Bar chart is gray value ratio of cleaved-caspase-3/caspase-3 in renal tissue of each group (n=5). [#]P<0.05, [##]P<0.01 vs. the NC group; [*]P<0.05, [**]P<0.01 vs. the cisplatin group. YSJZD, Yishen Jiangzhuo decoction; AKI, acute kidney injury; SIRT3, NAD-dependent deacetylase sirtuin-3; GSH, glutathione; SOD, superoxide dismutase; MDA, malondialdehyde TUNEL, TdT-mediated dUTP nick end labeling; NC, normal control; cl, cleaved.

reduce ROS accumulation in the kidneys (26,27). SOD, GSH and catalase production decrease when cisplatin enters renal tubular cells, eventually causing a build-up of ROS and an increase in MDA within the cells (5,6,8). The accumulation of cisplatin in the mitochondria of renal cells results in malfunction and damage, mostly manifesting as increased ROS generation (2,7,28). As the mitochondria are the main generators of ROS, SIRT3, a member of the NAD^{+}-dependent deacetylase family, may reduce ROS generation (29). The renoprotective benefits of the SIRT3-ROS pathway have also been demonstrated (30-33). YSJZD can downregulate TNF-α levels and upregulate the levels of SIRT3, GSH and SOD in the renal tissue, thus reducing ROS production. The mechanistic study was based on target genes screened using transcriptome sequencing; therefore, ROS detection in frozen sections of renal tissue could not be performed. YSJZD can significantly reduce MDA levels and alleviate mitochondrial damage in RTECs and may be able to reduce cisplatin-induced AKI induced by cisplatin in mice by preventing oxidative stress. Decreased ROS production leads to the downregulation of P38

MAPK phosphorylation and ultimately to decreased TNF-α production (5,22).

Renal tubular cell death is a common histopathological feature of cisplatin-induced nephrotoxicity (34). Cisplatin induces cell death via two primary mechanisms: Necrosis and apoptosis (35). Several apoptotic pathways have been implicated in the cisplatin-induced death of renal epithelial cells, including the endoplasmic reticulum stress-driven apoptosis and the intrinsic (mitochondrial) and extrinsic death receptor pathways through TNF-α generation (5,36). The activation of one or more of the three apoptotic pathways causes caspase-3 cleavage. The present study found that the cleaved-caspase-3/caspase-3 ratio and the number of TUNEL-positive cells per field were significantly lower in the cisplatin + YSJZD group than in the cisplatin group. The NF-κB signaling pathway can regulate the apoptotic pathways in renal tubular epithelial cells, enhancing the expression of downstream apoptosis-related genes, inducing apoptosis in these cells, thereby accelerating cell death and shedding and contributing to the development of AKI.

YSJZD significantly decreased the expression level of TNF-α, thus reducing the apoptosis of cisplatin-induced RTECs. Decreased p38 activation reduces activation of downstream proteins and caspase-3 (36). YSJZD demonstrated a protective effect by decreasing oxidative stress and downstream consequences, such as RTECs apoptosis in cisplatin-induced AKI. These results showed that YSJZD considerably reduced cisplatin-induced apoptosis of renal tubular epithelial cells in AKI mice.

There are some limitations in this study. First, only WB is used to detect inflammatory factors. In subsequent experiments, newer and more targeted experimental techniques will be used to detect inflammatory factors to increase the reliability of data. Second, there was no liver toxicity in short-term application of YSJZD in this study. However, data on long-term hepatotoxicity are not available, so the long-term side effects of drugs will be monitored carefully in the subsequent studies. Third, because the verification is based on differentially expressed genes in transcriptomics, the present study did not detect JNK and ERK in MAPK signal pathway. The MAPK pathway will be the focus of subsequent studies to investigate the pharmacodynamic mechanism. The pathogenesis of cisplatin-induced AKI is complex and compound Chinese medicine has multiple targets; therefore, the core pharmacodynamic target gene pathway of YSJZD has not been completely elucidated in the present study.

Overall, the results of the present study showed that YSJZD was an effective drug for the treatment of cisplatin-induced AKI. The main target genes of YSJZD include markers of oxidative stress, such as SIRT3, and markers of inflammation and apoptosis, such as TNF-α, p65 and p38 MAPK. These findings provide a theoretical and experimental foundation for the use of YSJZD to prevent cisplatin-induced AKI.

Acknowledgements

Not applicable.

Availability of data and materials

The data generated in the present study may be requested from the corresponding author. The raw RNA-seq data that support the findings were deposited in the gene expression omnibus (GEO) repository with an accession no. GSE262792 (https://www.ncbi.nlm.nih.gov/geo/query/acc.cgi?acc=GSE262792).

Authors' contributions

DZ and SR contributed to the conception of the study and design of the experiments. DZ, XR and YQ performed the experiments. DZ, XR, QW and YQ analyzed and interpreted the data. DZ, XR, QW and SR wrote and revised the manuscript. DZ and SR confirm the authenticity of all the raw data. All authors read and approved the final manuscript.

Ethics approval and consent to participate

The protocol of the present study was reviewed and approved by the Fujian University of Traditional Chinese Medicine Laboratory Animal Welfare and Ethics Committee, approval no. FJ-TCM IACUC2020021.

Patient consent for publication

Not applicable.

Competing interests

The authors declare that they have no competing interests.

References

1. Zhang Q, Qi J, Luo Q, Wu M, Zhang L, Qin L and Nie X: Yishen Xiezhuo formula ameliorates the development of cisplatin-induced acute kidney injury by attenuating renal tubular epithelial cell senescence. Ann Transl Med 10: 1392, 2022.
2. Volarevic V, Djokovic B, Jankovic MG, Harrell CR, Fellabaum C, Djonov V and Arsenijevic N: Molecular mechanisms of cisplatin-induced nephrotoxicity: a balance on the knife edge between renoprotection and tumor toxicity. J Biomed Sci 26: 25, 2019.
3. Oliveira BM, de Almeida LF, Deluque AL, Souza CS, Maciel ALD, Francescato HDC, Costa RS, Giovanini C, de Paula FJA and Coimbra TM: Calcitriol reduces the inflammation, endothelial damage and oxidative stress in AKI caused by cisplatin. Int J Mol Sci 23: 15877, 2022.
4. Lu L, Liu W, Li S, Bai M, Zhou Y, Jiang Z, Jia Z, Huang S, Zhang A and Gong W: Flavonoid derivative DMXAA attenuates cisplatin-induced acute kidney injury independent of STING signaling. Clin Sci (Lond) 137: 435-452, 2023.
5. McSweeney KR, Gadanec LK, Qaradakhi T, Ali BA, Zulli A and Apostolopoulos V: Mechanisms of cisplatin-induced acute kidney injury: Pathological mechanisms, pharmacological interventions and genetic mitigations. Cancers (Basel) 13: 1572, 2021.
6. Holditch SJ, Brown CN, Lombardi AM, Nguyen KN and Edelstein CL: Recent advances in models, mechanisms, biomarkers and interventions in cisplatin-induced acute kidney injury. Int J Mol Sci 20: 3011, 2019.
7. Qi L, Luo Q, Zhang Y, Jia F, Zhao Y and Wang F: Advances in toxicological research of the anticancer drug cisplatin. Chem Res Toxicol 32: 1469-1486, 2019.
8. Fang CY, Lou DY, Zhou LQ, Wang JC, Yang B, He QJ, Wang JJ and Weng QJ: Natural products: Potential treatments for cisplatin-induced nephrotoxicity. Acta Pharmacol Sin 42: 1951-1969, 2021.
9. Mapuskar KA, Steinbach EJ, Zaher A, Riley DP, Beardsley RA, Keene JL, Holmlund JT, Anderson CM, Zepeda-Orozco D, Buatti JM, *et al*: Mitochondrial superoxide dismutase in cisplatin-induced kidney injury. Antioxidants (Basel) 10: 1329, 2021.
10. Sears SM and Siskind LJ: Potential therapeutic targets for cisplatin-induced kidney injury: Lessons from other models of AKI and Fibrosis. J Am Soc Nephrol 32: 1559-1567, 2021.
11. Xu YF, Ruan SW, Lin JM and Zhang Z: Yishen Jiangzhuo Granules affect tubulointerstitial fibrosis via a mitochondrion-mediated apoptotic pathway. Chin J Integr Med 21: 928-937, 2015.
12. Xu SY, Bian RL and Chen X: Experimental methodology of Pharmacology. People's Medical Publishing House, Beijing, 2002.
13. Zhang Y, Chang Y, Han Z, Ma K, Zeng X and Li L: Estrogen protects against renal ischemia-reperfusion injury by regulating Th17/Treg cell immune balance. Dis Markers 2022: 7812099, 2022.
14. Ranasinghe R, Mathai ML and Zulli A: Cisplatin for cancer therapy and overcoming chemoresistance. Heliyon 8: e10608, 2022.

15. Xu Z, Zhang M, Wang W, Zhou S, Yu M, Qiu X, Jiang S, Wang X, Tang C, Li S, *et al*: Dihydromyricetin attenuates cisplatin-induced acute kidney injury by reducing oxidative stress, inflammation and ferroptosis. Toxicol Appl Pharmacol 473: 116595, 2023.
16. Chou YN, Lee MM, Deng JS, Jiang WP, Lin JG and Huang GJ: Water extract from brown strain of *flammulina velutipes* alleviates cisplatin-induced acute kidney injury by attenuating oxidative stress, inflammation, and autophagy via PI3K/AKT pathway regulation. Int J Mol Sci 24: 9448, 2023.
17. Linkermann A, Bräsen JH, Darding M, Jin MK, Sanz AB, Heller JO, De Zen F, Weinlich R, Ortiz A, Walczak H, *et al*: Two independent pathways of regulated necrosis mediate ischemia-reperfusion injury. Proc Natl Acad Sci USA 110: 12024-12029, 2013.
18. Perse M and Veceric-Haler Z: Cisplatin-induced rodent model of kidney injury: Characteristics and challenges. Biomed Res Int 2018: 1462802, 2018.
19. Ozkok A, Ravichandran K, Wang Q, Ljubanovic D and Edelstein CL: NF-κB transcriptional inhibition ameliorates cisplatin-induced acute kidney injury (AKI). Toxicol Lett 240: 105-113, 2016.
20. Kim C, Kwak W, Won DH, Kim J, Hwang DB, Kim N, Kang M, Jeon Y, Park YI, Park JW and Yun JW: Loss of Dact2 alleviates cisplatin-induced nephrotoxicity through regulation of the Igfl-MAPK pathway axis. Cell Biol Toxicol 39: 3197-3217, 2023.
21. Yuan H, Zhao Y, Li S, Qin J and Yu X: Madecassoside ameliorates cisplatin-induced nephrotoxicity by inhibiting activation of the mitogen activated protein kinase pathway. Environ Toxicol 38: 1473-1483, 2023.
22. Ramesh G and Reeves WB: p38 MAP kinase inhibition ameliorates cisplatin nephrotoxicity in mice. Am J Physiol Renal Physiol 289: F166-F174, 2005.
23. Ramesh G and Reeves WB: TNF-alpha mediates chemokine and cytokine expression and renal injury in cisplatin nephrotoxicity. J Clin Invest 110: 835-842, 2002.
24. Zhang B, Ramesh G, Norbury CC and Reeves WB: Cisplatin-induced nephrotoxicity is mediated by tumor necrosis factor-alpha produced by renal parenchymal cells. Kidney Int 72: 37-44, 2007.
25. Ramesh G, Kimball SR, Jefferson LS and Reeves WB: Endotoxin and cisplatin synergistically stimulate TNF-alpha production by renal epithelial cells. Am J Physiol Renal Physiol 292: F812-F819, 2007.
26. Pan Y, Zhang Y, Li J, Zhang Z, He Y, Zhao Q, Yang H and Zhou P: A proteoglycan isolated from Ganoderma lucidum attenuates diabetic kidney disease by inhibiting oxidative stress-induced renal fibrosis both in vitro and in vivo. J Ethnopharmacol 310: 116405, 2023.
27. Lu XH, Zhang J and Xiong Q: Suppressive effect erythropoietin on oxidative stress by targeting AMPK/Nox4/ROS pathway in renal ischemia reperfusion injury. Transpl Immunol 72: 101537, 2022.
28. Ma Q, Xu Y, Tang L, Yang X, Chen Z, Wei Y, Shao X, Shao X, Xin Z, Cai B, *et al*: Astragalus polysaccharide attenuates cisplatin-induced acute kidney injury by suppressing oxidative damage and mitochondrial dysfunction. Biomed Res Int 2020: 2851349, 2020.
29. Yang L, Wang B, Guo F, Huang R, Liang Y, Li L, Tao S, Yin T, Fu P and Ma L: FFAR4 improves the senescence of tubular epithelial cells by AMPK/SirT3 signaling in acute kidney injury. Signal Transduct Target Ther 7: 384, 2022.
30. Huang Z, Li Q, Yuan Y, Zhang C, Wu L, Liu X, Cao W, Guo H, Duan S, Xu X, *et al*: Renalase attenuates mitochondrial fission in cisplatin-induced acute kidney injury via modulating sirtuin-3. Life Sci 222: 78-87, 2019.
31. Li Y, Ye Z, Lai W, Rao J, Huang W, Zhang X, Yao Z and Lou T: Activation of sirtuin 3 by silybin attenuates mitochondrial dysfunction in cisplatin-induced acute kidney injury. Front Pharmacol 8: 178, 2017.
32. Morigi M, Perico L, Rota C, Longaretti L, Conti S, Rottoli D, Novelli R, Remuzzi G and Benigni A: Sirtuin 3-dependent mitochondrial dynamic improvements protect against acute kidney injury. J Clin Invest 125: 715-726, 2015.
33. Zi Y, Wang X, Zi Y, Yu H, Lan Y, Fan Y, Ren C, Liao K and Chen H: Cigarette smoke induces the ROS accumulation and iNOS activation through deactivation of Nrf-2/SIRT3 axis to mediate the human bronchial epithelium ferroptosis. Free Radic Biol Med 200: 73-86, 2023.
34. Wen L, Wei Q, Livingston MJ, Dong G, Li S, Hu X, Li Y, Huo Y and Dong Z: PFKFB3 mediates tubular cell death in cisplatin nephrotoxicity by activating CDK4. Transl Res 253: 31-40, 2023.
35. Lee D, Yamabe N, Lee H, Lim Lee H, Kim DW, Wook Lee J and Sung Kang K: Necrostatins regulate apoptosis, necroptosis, and inflammation in cisplatin-induced nephrotoxicity in LLC-PK1 cells. Bioorg Med Chem Lett 48: 128256, 2021.
36. Oh GS, Kim HJ, Shen A, Lee SB, Khadka D, Pandit A and So HS: Cisplatin-induced kidney dysfunction and perspectives on improving treatment strategies. Electrolyte Blood Press 12: 55-65, 2014.